Catalysis Today 139 (2008) 15–23

Contents lists available at ScienceDirect

Catalysis Today

journal homepage: www.elsevier.com/locate/cattod

Complete oxidation of *o*-xylene over Pd/Al_2O_3 catalyst at low temperature

Shaoyong Huang, Changbin Zhang, Hong He *

Research Center for Eco-Environmental Sciences, Chinese Academy of Sciences, P.O. Box 2871, 18 Shuangqing Road, Beijing 100085, PR China

ARTICLE INFO

Article history:
Available online 18 September 2008

Keywords:
o-Xylene catalytic oxidation
Noble metal catalyst
Pd/Al_2O_3
Mechanism

ABSTRACT

The catalytic activities of γ-Al_2O_3 supported noble metal (Pd, Pt, Au, Ag, Rh) catalysts were tested and compared for catalytic oxidation of *o*-xylene. The results show that Pd/Al_2O_3 is the most active catalyst among these noble metal catalysts. The effects of Pd loading and gas hourly space velocity (GHSV) on the activity of Pd/Al_2O_3 catalyst for *o*-xylene oxidation were investigated at low temperature from 60 to 190 °C. At 1 wt% Pd loading, 100 ppm *o*-xylene can be completely oxidized to CO_2 and H_2O at ca.110 °C over the Pd/Al_2O_3 catalyst at a GHSV of 10,000 h^{-1}. The 1% Pd/Al_2O_3 was characterized using BET, XRD methods. The XRD patterns showed that PdO was the dominant species in the fresh Pd/Al_2O_3 catalyst and metallic Pd was the main phase in both the H_2 pretreated and the used catalysts. The metallic Pd is proposed to be the active species for *o*-xylene oxidation. The mechanism of *o*-xylene oxidation was studied with respect to the behavior of adsorbed species on Pd/Al_2O_3 surface examined by in situ DRIFTS and the gas products detected by the online GC/MS. On the basis of experimental results, a simplified mechanism for the catalytic oxidation of *o*-xylene over Pd/Al_2O_3 was proposed.

1. Introduction

Volatile organic compounds (VOCs) are considered as a major pollutant in indoor and outdoor air. They also contribute to the formation of photochemical smog and destruction of ozone layer. BTX (benzene, toluene, xylene), as one of the major VOCs exist in air in a large scale. These aromatic compounds can be produced from a variety of industrial and commercial process. The BTX are of particular concern due to their high toxic potential for human beings [1,2].

There are many different techniques available to remove VOCs from the polluted air. Among these techniques, the catalytic oxidation is considered as an effective way due to higher destructive efficiency, lower operating temperature, lower NO_x emissions than thermal combustion systems, especially for low concentration of VOCs. During the last decades, the complete oxidation of VOCs has been widely studied over either supported noble metals or metal oxides catalysts in view of developing catalytic oxidation applications [3–7]. The advantages of noble metal catalysts over metal oxides include superior specific activity and high selectivity, which makes them as the best candidates for low temperature complete oxidation of VOCs. The mostly studied noble metals are Pt and Pd, either singly or as a bi-metallic catalyst. The supports used are metal oxides, activated carbon and zeolite, etc. In the case of metal oxide supported Pt and Pd catalyst, the commonly used supports are Al_2O_3, ZrO_2, CeO_2, SiO_2 and TiO_2 and so on [3,8–10]. With the metal oxide supported Pt and Pd catalysts, most of the reaction temperatures for 100% conversion of BTX were above 200 °C. Over zeolite supported Pt and Pd catalyst, the 1000 ppm xylene could be completely removed at a similar temperature with the metal oxide supported catalyst [11,12]. Due to the hydrophobic surface, the activated carbon supported Pt and Pd catalysts showed the highest activity for BTX total oxidation in all of the published issues, and the 100% BTX conversion could be achieved at a temperatures as low as 140 °C at a GHSV of 21,000 h^{-1} [7]. However, it is difficult for this catalyst to be washcoated on a honeycomb support when applied in practice.

Compared with the supported Pt catalyst, the supported Pd catalyst shows some advantages. On the one hand, Pd displays a better resistance to thermal and hydrothermal sintering than that of Pt [13]. On the other hand, Pd is cheaper than Pt. Therefore, the choice of Pd as the active component rather than Pt is essentially determined on the basis of stability and economy considerations. Pd/Al_2O_3, as a commercial catalyst, has been extensively investigated for catalytic oxidation of VOCs, especially for methane oxidation, whereas the studies on benzene series catalytic oxidation, especially on xylene, are relatively scarce.

* Corresponding author. Tel.: +86 10 62849123; fax: +86 10 62923563.
E-mail address: honghe@rcees.ac.cn (H. He).

0920-5861/$ – see front matter © 2008 Elsevier B.V. All rights reserved.
doi:10.1016/j.cattod.2008.08.020

Although the complete oxidation mechanism of aromatic compounds had been investigated formerly, the detailed reaction mechanism still needs to be proposed. Marsh et al. [14,15] have investigated the mechanism of benzene oxidation on the Pt (1 1 1) surface using temperature-programmed reaction spectroscopy (TPRS) and in situ soft X-ray methods respectively in a high vacuum condition. In their studies, they found that C–H and C–C bond activation were clearly rate-limiting steps for the benzene oxidation on the Pt (1 1 1) surface and the reaction proceeded through four surface adsorbed intermediates: η^6-benzene, 1,4-di-σ-2,5-cyclohexadiene, 1,1,4-tri-σ-2,5-cyclohexadiene and η^5-cyclohexadiene. By employing an in situ FTIR technique, Lichtenberger et al. [16] have studied the catalytic oxidation mechanism of chlorinated benzene over V_2O_5/TiO_2 catalyst. They found that C–Cl bond scission is the first step of the oxidation of chlorobenzene, and the activation of chlorinated aromatic compounds is easier than that of benzene. The *o*-benzoquinone, catecholate, *p*-benzoquinone, maleates, acetates and aldehydes were detected in their studies. The CO, CO_2 and H_2O were the major reaction productions. Selvaraj et al. [17] have investigated the mechanism of xylene partial oxidation over mesoporous molecular sieves catalyst V-Mo-MCM-41 using GC/MS and they found the tolualdehyde is the reaction intermediate and the maleic anhydride and phthalide are the side products in the reaction. However, all these studies could not be properly applied to the *o*-xylene catalytic oxidation over γ-Al_2O_3 supported noble metal catalysts under atmosphere conditions.

The aim of this work is to study the activities of γ-Al_2O_3 supported noble metal catalysts (Pd, Pt, Ag, Rh, Au) for catalytic oxidation of *o*-xylene and propose a reaction mechanism for *o*-xylene catalytic oxidation over Pd/Al_2O_3 catalyst.

2. Experimental

2.1. Catalyst preparation

The Al_2O_3 supported noble metal (Pd, Pt, Rh, Au and Ag) catalysts were prepared via the wet impregnation technique with γ-Al_2O_3 and an aqueous solution containing appropriate amount of $Pd(NO_3)_2$, H_2PtCl_6, $RhCl_3$, $AuCl_3$ and $AgNO_3$, respectively. The amount of solvent was added by a ratio of 10 mL per gram of support. After stirring for 3 h, the excessive water was removed in a rotary evaporator at 60 °C. The samples were dried overnight at 110 °C and calcined at 500 °C for 3 h in air to decompose the metal salt adsorbed on the γ-Al_2O_3 support. Then, the prepared catalyst was crushed and sieved to 40–60 mesh for use, which was defined as fresh catalyst. Prior to the activity testing or characterization, the fresh catalyst was pre-reduced at 300 °C for 1 h in pure hydrogen at a flow rate of 30 mL min^{-1}.

2.2. Activity test of catalysts

The activity tests for catalytic oxidation of *o*-xylene over the supported noble metal catalysts were preformed in a continuous-flow fixed bed reactor under atmospheric pressure. The catalyst (40–60 mesh) was supported on a small plug of glass wool in the middle of a straight-tube Pyrex reactor. The 100 ppm *o*-xylene gas was produced by a N_2 stream bubbling through a saturator filled with liquid *o*-xylene and the concentration of *o*-xylene was controlled by either the flow of rate nitrogen or temperature of water bath which was kept at 0 °C. The reaction feed consisted of 100 ppm *o*-xylene and 20% O_2 in N_2. The flow rate of the gas mixture through the reactor was 100 mL min^{-1}. The reactants and the products were analyzed on-line using a GC/MS (Hewlett-Packard 6890N gas chromatograph interfaced to a Hewlett-Packard 5973N mass selective detector) with a HP-5MS capillary column (30 m × 0.25 mm × 0.25 μm) and another GC (Shangfen, GC112A) with a carbon molecule sieve column.

2.3. Characterization of catalyst

The BET surface areas were determined in a Quantasorb-18 automatic equipment by physical adsorption measurements with N_2 at −196 °C. Before measurement, the samples were originally outgassed at 300 °C for 4 h. The crystal phases of the catalysts were characterized by X-ray diffractometry using a computerized Rigaku D/max-RB X-ray diffractometry (Japan, Cu Kα radiation, 0.154056 nm) with the X-ray tube operated at 40 kV and 100 mA. TEM images were obtained by employing a JEOL-2010 device with 200 kV acceleration voltage.

2.4. In situ DRIFTS

In situ diffuse reflectance infrared Fourier transform spectroscopy (DRIFTS) spectra were recorded on a NEXUS 670 (Thermo Nicolet Instrument Corporation) FTIR, equipped with an in situ diffuse reflection chamber and a high-sensitivity mercury cadium telluride (MCT-A) detector cooled by liquid nitrogen. The sample (ca. 12 mg) for the in situ DRIFTS studies was finely ground and placed into a ceramic crucible in the in situ chamber. In experiments all of the spectra were recorded by collecting 100 scans with a resolution of 4 cm^{-1} from 650 to 4000 cm^{-1}. The reaction feed and total flow rate were consistent with those of catalyst test section.

2.5. o-Xylene TPO

o-Xylene temperature-programmed oxidation (TPO) was performed through a fixed-bed reactor. This reactor consisted of a 0.6-cm-OD quartz tube with a 0.5-mm-OD thermocouple placed in the center of a bed of 40–60 mesh catalyst particles (0.15 g). The thermocouple measured the temperature and provided feedback to the temperature programmer, which regulated heating of the electric furnace. A Hiden HPR 20 quadruple mass spectrometer detected products immediately downstream of the reactor as they were desorbed from the catalyst, and a computer allowed multiple signals and the thermocouple output to be recorded, simultaneously. After saturated adsorption of *o*-xylene at 50 °C, the samples were purged in He flow (50 mL/min) for 1 h, and then the temperature was increased from 50 to 400 °C at a heating rate of 20 °C/min in a flow of 20% O_2 in He while the temperature and desorption products were recorded.

3. Results and discussion

3.1. Catalytic activity and characterization of catalysts

3.1.1. Effect of noble metals

The catalytic activities of γ-Al_2O_3 supported noble metal (Pd, Pt, Rh, Ag, Au) catalysts were performed for catalytic oxidation of *o*-xylene and the results were shown in Fig. 1. The 1 wt% Pd/Al_2O_3 catalyst showed the best activity and *o*-xylene conversion reached 90% at ca. 160 °C at a GHSV of 50,000 h^{-1}, while for the Pt, Ag, Rh and Au catalysts the conversion was less than 40% at 200 °C. The activities of these catalysts followed the order of $Pd/Al_2O_3 > Pt/Al_2O_3 > Ag/Al_2O_3 > Rh/Al_2O_3 > Au/Al_2O_3$. It is worthwhile to note that in these reaction conditions, the activity of Pd/Al_2O_3 was much higher than that of the Pt/Al_2O_3, which is inconsistent with the result that platinum is the most active metal for hydrocarbon oxidation, except for methane [10,18]. Some studies also showed

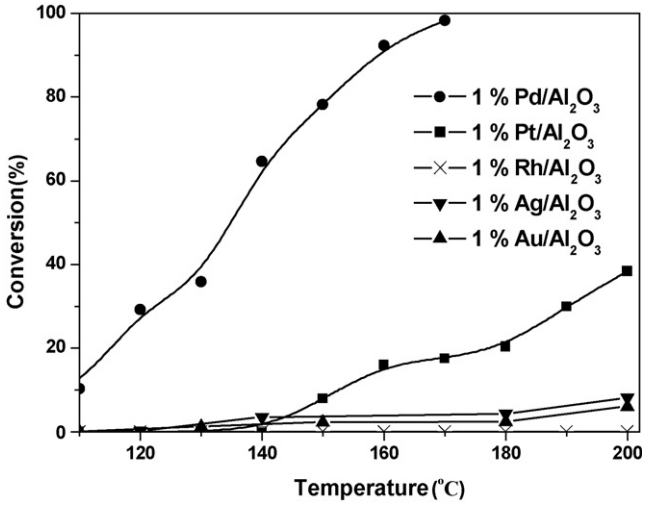

Fig. 1. *o*-Xylene conversions of Al_2O_3 supported 1% noble metal catalysts at various temperatures. Reaction conditions: *o*-xylene 100 ppm, 20% O_2/N_2 balance, total flow rate 100 mL min^{-1}, GHSV 50,000 h^{-1}.

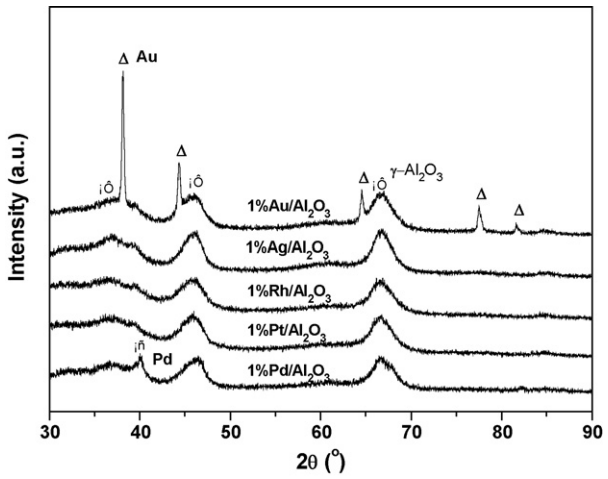

Fig. 2. X-ray diffraction patterns of γ-Al_2O_3 supported noble metal catalysts.

that the residual chlorine coming from the precursor during the preparation has some negative effect on the catalyst activity for VOCs oxidation [19,20]; however, it just has a minor effect on the catalyst activity in our experimental conditions (result not shown).

The BET surface areas of γ-Al_2O_3 and Al_2O_3 supported noble metal catalysts were measured, and the results were given in Table 1. It shows that deposit of 1 wt% noble metal on γ-Al_2O_3 support had no obvious effects on the surface areas changes. That is, the variations in the surface areas of these catalysts can be considered as a negligible factor for the different catalytic activities of *o*-xylene oxidation.

The crystal structures of γ-Al_2O_3 supported noble metal catalysts were revealed by XRD. Fig. 2 shows that only the diffraction lines of γ-Al_2O_3 ($2\theta = 37.7°$, 45.9°, 66.9° PDF 79-1558) appeared in the XRD patterns of the 1 wt% supported Pt, Ag and Rh catalysts. The absence of diffraction lines of Pt ($2\theta = 39.8°$, 46.2°, 67.5°, 40.6° PDF 65-2868), Ag ($2\theta = 38.1°$, 44.3°, 64.4°, 77.4° PDF 65-2871) and Rh ($2\theta = 41.1°$, 47.8°, 69.9°, 84.4° PDF 05-0685) indicates that the Pt, Ag and Rh are well dispersed on the γ-Al_2O_3 support. In the XRD patterns of Au/Al_2O_3 and Pd/Al_2O_3 catalysts, the diffraction lines of Au ($2\theta = 38.2°$, 44.4°, 64.6°, 77.6° PDF 65-2870) and Pd ($2\theta = 40.2°$, 46.8°, 68.3° PDF 87-0639) were detected. The Au particles are about 35 nm (calculated by using Scherrer equation), which is much bigger than its optimal size (ca. 3 nm) for catalytic oxidation [21,22]. For Pd catalyst, the Pd microcrystal is less than 10 nm.

3.1.2. Effect of the Pd loading

Based on the above results, we focused the studies on the supported Pd catalyst for catalytic oxidation of *o*-xylene. To examine the influence of Pd loading on the catalytic activity of Pd/Al_2O_3, experiments were carried out by varying Pd loading from 0.5 to 6 wt%. The results were given in Fig. 3. The results show that the *o*-xylene conversion increased with the increasing of Pd loading on the Pd/Al_2O_3 catalyst. The 6 wt% Pd/Al_2O_3 was proved to be the most active catalyst for catalytic oxidation of *o*-xylene. The 90% conversion was obtained at ca. 145 °C with a total flow rate of 100 mL min^{-1} at GHSV of 50,000 h^{-1}. The BET results (in Table 2) show that just small changes were detected among the supported Pd catalysts with various Pd loadings, indicating the BET has a negligible effect on the activities of different Pd loadings catalysts. The XRD patterns (in Fig. 4) show that the intensity of Pd diffraction lines increased with the Pd loading varying from 0.5% to 6% and no PdO diffraction lines ($2\theta = 33.5°$, 33.8°, 54.7°) were detected. The average particle sizes of Pd particles obtained from the TEM images were found to change from ca. 10 to 20 nm with the increase of the Pd loading as shown in Table 2. Fig. 5 shows that aggregation of Pd particles was observed in high Pd loading catalyst, especially in 6% Pd/Al_2O_3 catalyst. Therefore, we think that the enhanced catalytic activities could be due to the increase of the number of Pd active species in higher Pd loading catalysts, despite of the aggregation of the metallic Pd. Taking the activity and the economic factor into account, the 1 wt% Pd/Al_2O_3 was chosen as the target catalyst for the following researches.

Table 1
The surface areas of γ-Al_2O_3 and γ-Al_2O_3 supported noble metal catalysts

Sample	BET area (m^2 g^{-1})
γ-Al_2O_3	305
1% Pd/Al_2O_3	290
1% Pt/Al_2O_3	303
1% Rh/Al_2O_3	290
1% Au/Al_2O_3	283
1% Ag/Al_2O_3	287

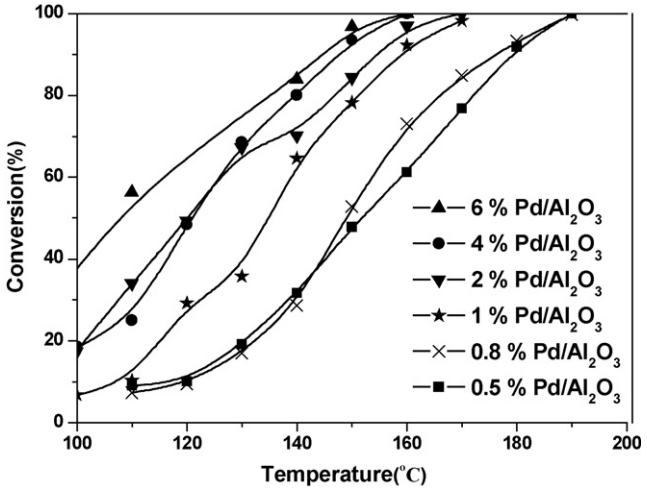

Fig. 3. *o*-Xylene conversions of Pd/Al_2O_3 catalysts with various Pd loadings. Reaction conditions: *o*-xylene 100 ppm, 20% O_2/N_2 balance, total flow rate 100 mL min^{-1}, GHSV 50,000 h^{-1}.

Table 2
The surface areas of Pd/Al_2O_3 catalysts with different Pd loadings

Sample	BET area ($m^2\ g^{-1}$)	Particle size (nm)
0.5% Pd/Al_2O_3	295	9.0
0.8% Pd/Al_2O_3	293	9.6
1% Pd/Al_2O_3	290	9.1
2% Pd/Al_2O_3	305	10.0
4% Pd/Al_2O_3	292	12.5
6% Pd/Al_2O_3	280	19.3

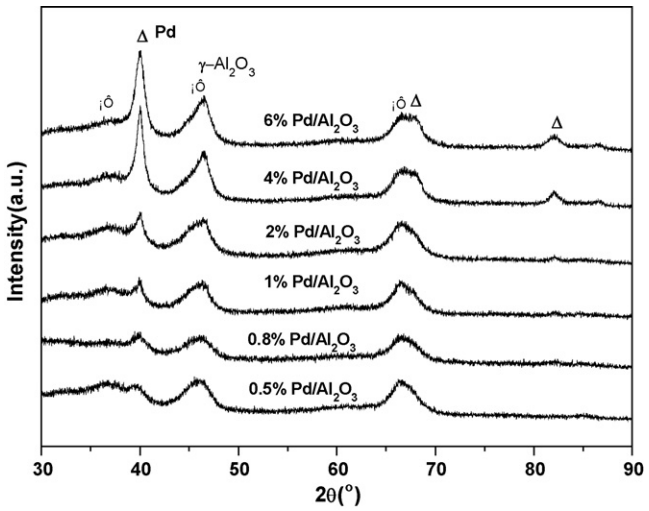

Fig. 4. X-ray diffraction patterns of Pd/Al_2O_3 catalysts with different loadings. Sample pretreatment conditions: H_2, flow rate 30 mL min^{-1}, 300 °C for 1 h.

3.1.3. Effect of GHSV

To investigate the influence of GHSV on *o*-xylene catalytic oxidation over the Pd/Al_2O_3 catalyst, the experiments were carried out at GHSVs of 10,000, 20,000, 50,000 and 100,000 h^{-1}, respectively by changing the volume of the catalyst. It is worth noting that in these experiments the gas flow rate (F) and the catalyst particle size was kept at a constant value. The only changed factor was the catalyst volume (υ). Therefore, the inner and outer diffusion of the reactant gave an identical effect on the catalytic activity at different GHSVs and the variation of the apparent reaction rate was totally influenced by the kinetics process. As can be seen from the Fig. 6, the GHSV has a significant effect on the catalytic activity of Pd/Al_2O_3 catalyst. The catalytic

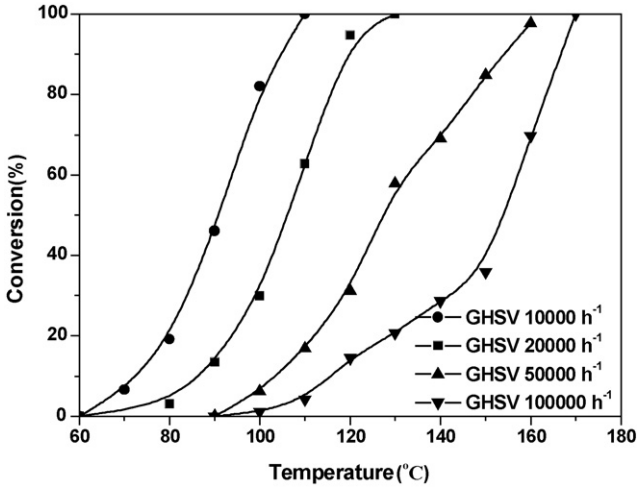

Fig. 6. *o*-Xylene conversions of 1% Pd/Al_2O_3 catalyst at various GHSVs. Reaction conditions: *o*-xylene 100 ppm, 20% O_2/N_2 balance, total flow rate 100 mL min^{-1}.

activity increased sharply with the decrease of the GHSVs, which could be explained as the decrease of the GHSVs results in the increase of residence time, therefore the catalytic activity was promoted. For instance, at the GHSV of 100,000 h^{-1}, 100 ppm *o*-xylene can be completely removed at ca. 170 °C, while at GHSVs of 50,000, and 20,000 h^{-1} the catalytic oxidation temperature decreased to 160 °C and 130 °C, respectively. It is worth noting that when using a GHSV of 10,000 h^{-1} the 100 ppm *o*-xylene can be completely removed at the temperature as low as 110 °C and this temperature is the lowest one for BTX catalytic oxidation in all of the studies issued by now.

3.1.4. Changes of Pd species during o-xylene catalytic oxidation

The crystal phases of Pd before and after the H_2 pretreatment and catalytic test were examined by XRD. Fig. 7 shows the XRD patterns of fresh (a), H_2 pretreated (b) and after test (c) Pd/Al_2O_3 catalysts. The diffraction lines at $2\theta = 37.7°$, 45.9° and 66.9° (PDF 79-1558) are assigned to γ-Al_2O_3 and those at $2\theta = 33.5°$, 33.8° and 54.7° (PDF 41-1107) are attributed to PdO species. The diffraction lines at $2\theta = 40.2°$, 46.8° and 68.3° (PDF 87-0639) are the characteristic of metallic Pd phase. As can be seen, PdO is the dominant phase in fresh catalyst which was calcined at 500 °C for 3 h in air and no metallic Pd diffraction lines were detected, however, the metallic Pd is the main species and no PdO phase appeared in both the H_2 pretreated and the used catalysts. This

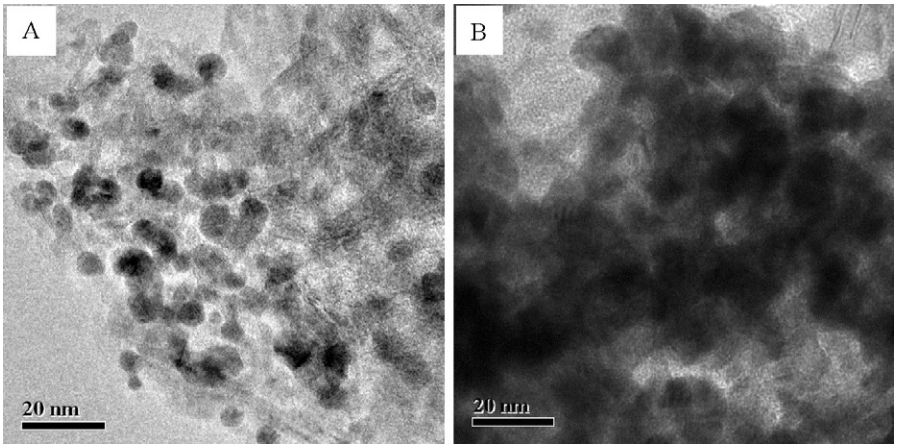

Fig. 5. TEM images of Pd/Al_2O_3 catalysts with various Pd loadings. (A) 1% Pd/Al_2O_3, (B) 6% Pd/Al_2O_3. Sample pretreatment conditions: H_2, flow rate 30 mL min^{-1}, 300 °C for 1 h.

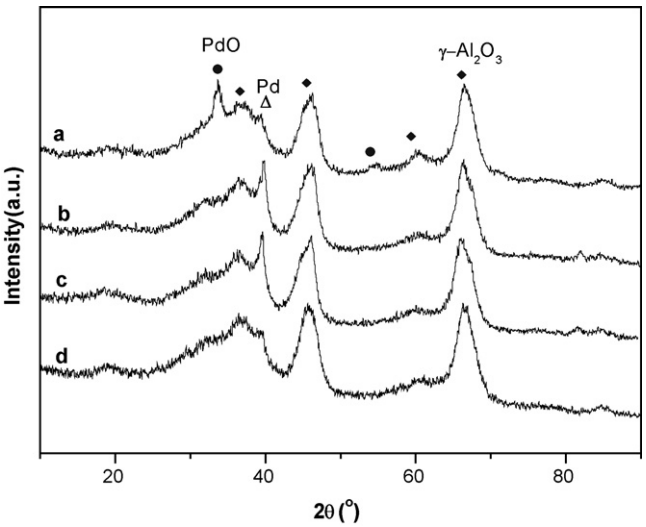

Fig. 7. X-ray diffraction patterns of 1% Pd/Al_2O_3 catalysts. (a) Fresh catalyst, (b) H_2 pretreated catalyst, (c) after test and (d) γ-Al_2O_3.

result suggests that the Pd species can be maintained in a metallic phase after the reaction due to the low reaction temperature (no more than 180 °C). Therefore, we propose that the metallic Pd species plays an important role for the catalytic oxidation of *o*-xylene over Pd/Al_2O_3 catalyst, and a further discussion about the active species of Pd/Al_2O_3 catalyst for *o*-xylene catalytic oxidation will be given in our next work.

3.1.5. Analysis of the reaction products

Analyses of the reaction products during *o*-xylene catalytic oxidation over Pd/Al_2O_3 catalyst were performed using the online GC and GC/MS. The results were given in Figs. 8 and 9. During the catalytic oxidation of *o*-xylene, CO_2 and H_2O were the major products and no CO was detected by the online GC. Fig. 8 shows the gap between the *o*-xylene conversion and CO_2 yield and the CO_2 yield could reach 100% at the reaction temperature of 180 °C. Compared the curves of *o*-xylene conversion and the CO_2 yield, we could conclude that some reaction intermediates must be formed during the oxidation of *o*-xylene below 180 °C. For confirmation of the gas reaction intermediates, the effluent gases were analyzed by employing the online GC/MS, as shown in Fig. 9(a–c). The results

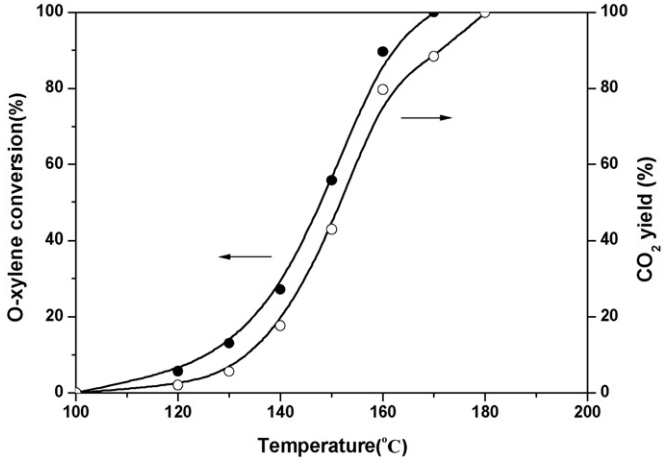

Fig. 8. The *o*-xylene conversion and CO_2 selectivity for *o*-xylene catalytic oxidation over 1% Pd/Al_2O_3 catalyst. Reaction conditions: *o*-xylene 100 ppm, 20% O_2/N_2 balance, total flow rate 100 mL min^{-1}, GHSV 50,000 h^{-1}.

indicate that a trace of organic intermediates including 2-methyl benzaldehyde (MW: 120, m/z = 91, 119, 120), 1(3H)-isobenzofuranone (MW: 134, m/z = 105, 77, 134), phthalic anhydride (MW: 148, m/z = 104, 76, 50) and maleic anhydride (MW: 98, m/z = 26, 54, 28) were formed from 130 to 160 °C during the catalytic oxidation of *o*-xylene. In Fig. 9(c), due to the high reactant concentrations, these intermediates were still detected above 180 °C, which denotes the total oxidation temperature of *o*-xylene increased with the rising of reactant concentration. Some species such as toluene, *m*-xylene, trimethylbenzene and methylethylbenzene also appeared in the mass spectra. These species were proved to be existed in the reactant and be produced by the isomerization or transalkylation of *o*-xylene. 2-Methyl benzaldehyde, 1(3H)-isobenzofuranone, phthalic anhydride and maleic anhydride species were considered as the intermediates in complete oxidation of *o*-xylene.

3.2. Catalytic reaction mechanism

In order to investigate the mechanism of *o*-xylene catalytic oxidation over Pd/Al_2O_3 catalyst, the DRIFTS experiments were performed. Fig. 10 shows the changes in the DRIFTS spectra of Pd/Al_2O_3 catalyst as a function of temperature in a flow of O_2 + *o*-xylene + N_2. After the catalyst was exposed to O_2 + *o*-xylene + N_2 mixture gas, several bands appeared during the reaction temperature rising from 30 to 250 °C. According to the previous studies, the negative band at 3745 cm^{-1} pertained to the stretching vibration of surface OH species (ν(OH)) on γ-Al_2O_3, which indicates that OH species was consumed during the reaction. The bands at 3070, 3016 cm^{-1} and 2970, 2941, 2883 cm^{-1} were assigned to the ν(C–H) of the aromatic ring and $-CH_3$, respectively [23,24]. Three weak bands at 1840, 1743 and 1261 cm^{-1} were ascribed to υ_{as}(O–C–O), υ_s(O–C–O) and υ(C–O–C) of acid anhydride species [25]. Bands at 1610, 1587, 1489 and 1465 cm^{-1} were attributed to the aromatic ring vibration of *o*-xylene and 1388 cm^{-1} was ascribed to the δ(C–H) of $-CH_3$, which is consistent with other researches [23,24,26,27]. Bands corresponding to $\nu_{as}(COO^-)$ and $\nu_s(COO^-)$) for carboxylate ($C \geq 2$) and formate species were detected at 1587, 1568, 1450 and 1370 cm^{-1} [28–31]. Bands due to the vibrations of bicarbonate species rose at 3630, 1653, and 1427 cm^{-1} [32,33].

When 100 ppm *o*-xylene mixture gas was introduced to Pd/Al_2O_3 at 30 °C, the adsorbed *o*-xylene (1610, 1587, 1489 and 1465 cm^{-1}) was detected immediately, and we also noticed that a negative peak of ν(OH) (at 3745 cm^{-1}) appeared, indicating the *o*-xylene molecules may be adsorbed on the catalyst surface through an interaction with the surface OH of the γ-Al_2O_3 support [34]. With the reaction temperature raised from 30 to 100 °C, the carboxylate species (1587, 1568, 1450 and 1370 cm^{-1}) such as formate, acetate, etc. were formed on the catalyst surface and increased rapidly with the rising temperature. Finally, these species became the dominant surface species on Pd/Al_2O_3 at ca. 100 °C. Meanwhile, the band intensities due to aromatic ring structure (1610, 1587, 1489 and 1465 cm^{-1}) increased, which denoted some species with an aromatic ring structure was still existed on the catalyst surface at this temperature. The orientation change of the adsorbed ring structure from parallel to tilt (vertical) [16,35,36] and/or more molecules with an aromatic ring structure adsorbed on the catalyst could contribute to the increase of intensity. Based on the results, we can conclude that the phthalate species was formed at this reaction temperature. When the reaction temperature was heated above 140 °C, the acid anhydride species (1840, 1743 and 1261 cm^{-1}) was detected. Taking into consideration of the increase in the IR adsorption intensity of aromatic ring and acid anhydride species, it can be deduced that

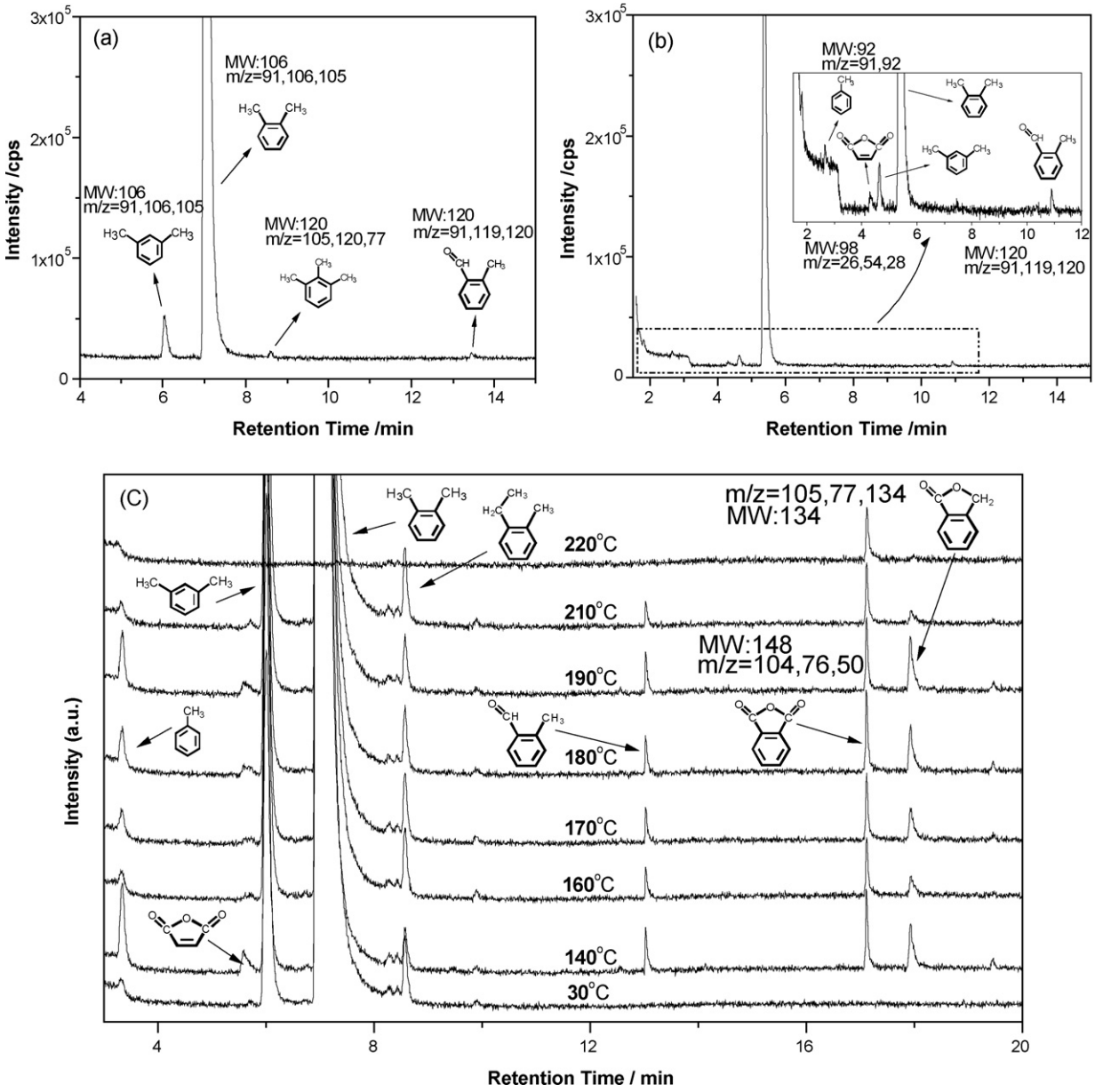

Fig. 9. GC/MS chromatograms for gaseous organic products of *o*-xylene total oxidation over 1% Pd/Al_2O_3 catalyst. Reaction conditions: 20% O_2/N_2 balance, total flow rate 100 mL min^{-1}, GHSV 50,000 h^{-1}, (a) for 100 ppm *o*-xylene at 130 °C, (b) for 100 ppm, *o*-xylene at 160 °C and (c) for 1000 ppm *o*-xylene at various reaction temperatures.

phthalic anhydride was generated over the Pd/Al_2O_3 catalyst. In the reaction temperature range from 140 to 250 °C, the bicarbonate species formed (3630, 1653, and 1427 cm^{-1}), and finally became the major peaks in the FTIR spectra. These species appeared at high temperature can be explained as follows, with the rising temperature more and more *o*-xylene molecules were oxidized to CO_2 through the catalytic oxidation, then the CO_2 transformed to bicarbonate species through the interaction with the surface OH group of the Pd/Al_2O_3 catalyst. The increase of the intensity of the negative OH vibration peak at 3745 cm^{-1} could be regarded as an evidence for the interaction between the gas CO_2 and the surface OH group of the γ-Al_2O_3 support.

In order to study the effect of γ-Al_2O_3 support on the reaction mechanism, *o*-xylene TPO tests were performed over the γ-Al_2O_3 support and the 1% Pd/Al_2O_3 catalyst and the result was shown in Fig. 11. Similar *o*-xylene TPO profiles were acquired over the γ-Al_2O_3 support (shown in Fig. 11A) and the 1% Pd/Al$_2$O catalyst (shown in Fig. 11B). The 1(3H)-isobenzofuranone (m/z = 105), phthalic anhydride (m/z = 104) and maleic anhydride (m/z = 26) species were detected during the *o*-xylene TPO over both the γ-Al_2O_3 support and the 1% Pd/Al_2O_3 catalyst, which denoted that these three intermediates were mainly produced by the catalysis of the γ-Al_2O_3 support. Only trace of CO_2 was detected during the *o*-xylene TPO over the γ-Al_2O_3 support under 300 °C. Consequently, we conclude that the partial oxidation of *o*-xylene took placed over the γ-Al_2O_3 support. However, over the 1% Pd/Al_2O_3 catalyst, a large amount of CO_2 was produced around 140 °C with the rising temperature, indicating that addition of 1% Pd into the γ-Al_2O_3 support resulted in the direct oxidation of the adsorbed *o*-xylene into CO_2 and H_2O through the interaction between the adsorbed *o*-xylene and oxygen on the metallic Pd [14,15]. The existence of the metallic Pd species also enhanced the complete oxidation of the intermediates to CO_2 and H_2O, according to the rapid decrease of the intermediates at about 140 °C in Fig. 11(B).

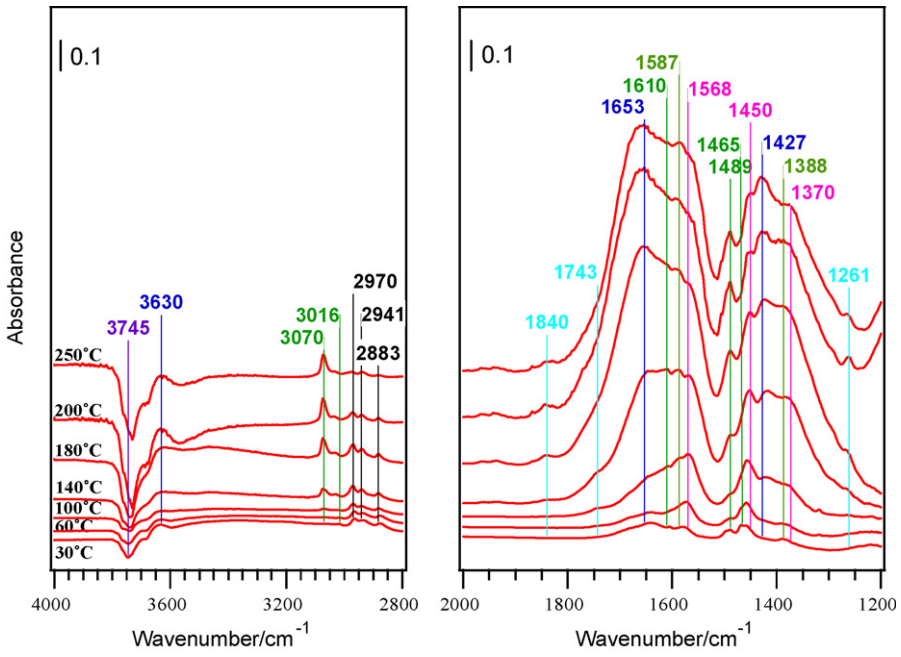

Fig. 10. In situ DRIFTS of *o*-xylene oxidation over 1% Pd/Al_2O_3 catalyst at different temperatures. Reaction conditions: *o*-xylene 100 ppm, total flow rate 100 mL min^{-1}, 20% O_2/N_2 balance.

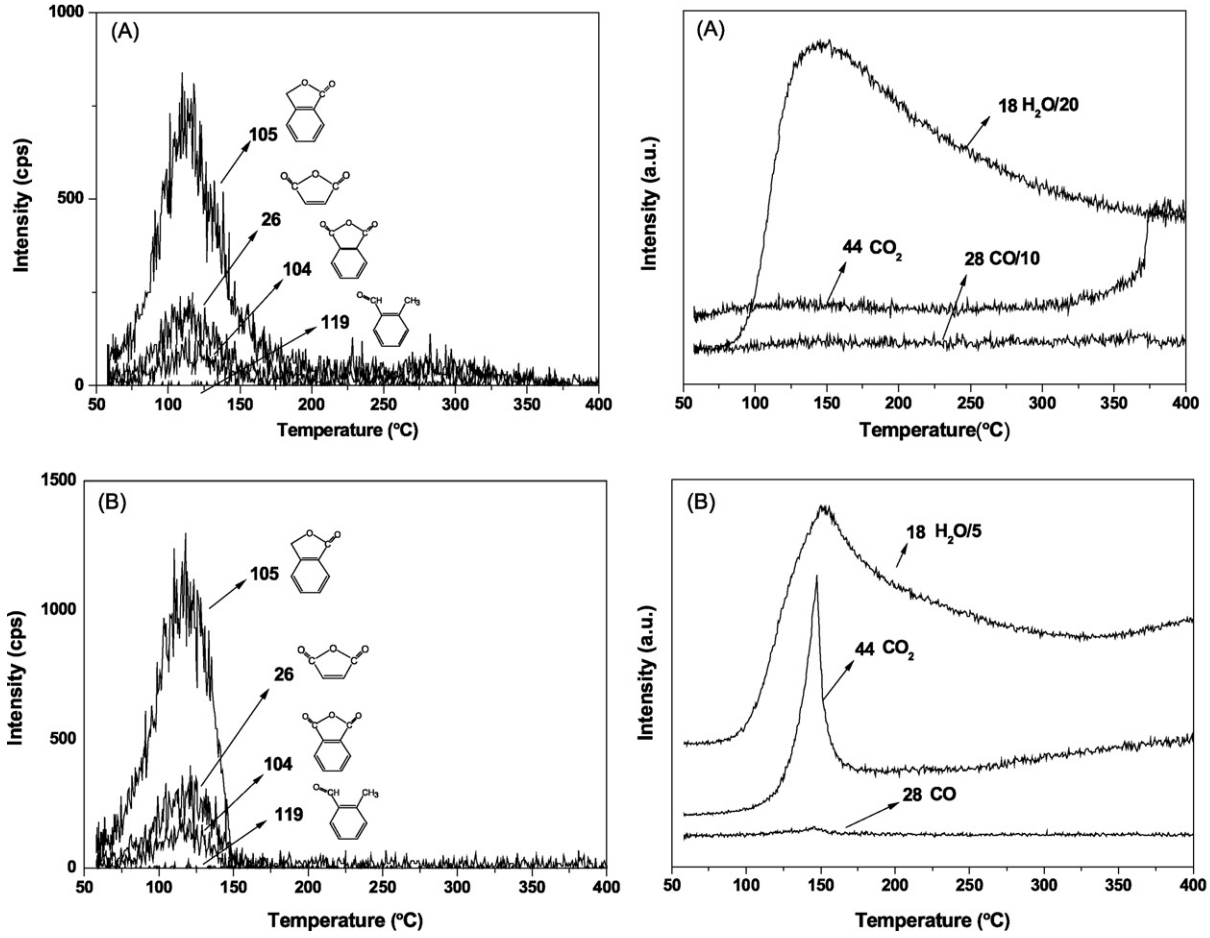

Fig. 11. *o*-Xylene TPO spectra over the γ-Al_2O_3 support and the 1% Pd/Al_2O_3 catalyst. *o*-Xylene TPO conditions: total flow rate 50 mL min^{-1}, 20% O_2/N_2 balance, heating rate 20 °C min^{-1}, (A) over γ-Al_2O_3 support and (B) over 1% Pd/Al_2O_3 catalyst.

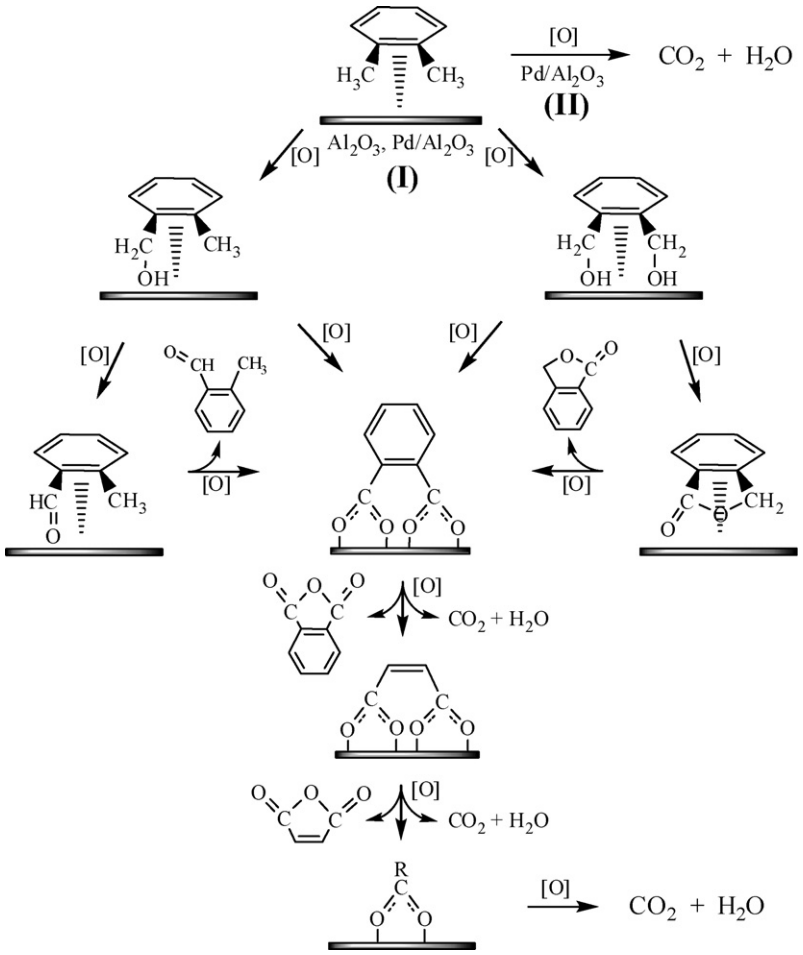

Fig. 12. The reaction scheme of the catalytic oxidation of *o*-xylene over 1% Pd/Al_2O_3 catalyst.

Fig. 12 gives two simplified reaction pathways for catalytic oxidation of *o*-xylene over Pd/Al_2O_3 catalyst. In the pathway I, the adsorbed *o*-xylene molecules were oxidized to benzyl alcohol species, and then generated 2-methyl benzaldehyde, 1(3H)-isobenzofuranone or phthalate via a rapid oxidation. The 2-methyl benzaldehyde, 1(3H)-isobenzofuranone could be further oxidized to phthalate species. After that, the adsorbed phthalate species was converted to surface maleate by breaking the ring structure. The adsorbed maleate species was oxidized to the surface carboxylate (formate/acetate) species. Finally, the goal targets CO_2 and H_2O were produced by the decomposition and the further oxidation of the surface carboxylate species, and this process mainly took place over the γ-Al_2O_3 support. In the reaction pathway II, the *o*-xylene molecules adsorbed on the metallic Pd were oxidized directly into CO_2 and H_2O through the interaction between the adsorbed *o*-xylene and oxygen. In catalytic oxidation of *o*-xylene, the 2-methyl benzaldehyde, 1(3H)-isobenzofuranone, phthalic anhydride and maleic anhydride were detected in the desorbed products (Figs. 9 and 11), and the surface phthalate, maleate and carboxylate (formate/acetate) species were recognized by the in situ DRIFTS (Fig. 10). The catalytic oxidation of *o*-xylene over the Pd/Al_2O_3 is more complicated than the above discussion, and a further investigation will be given in our future work.

4. Conclusions

Among the γ-Al_2O_3 supported noble metal (Pd, Pt, Au, Ag, Rh) catalysts, Pd/Al_2O_3 is found to be the most active catalyst for the complete oxidation of *o*-xylene. The catalytic activities of Pd/Al_2O_3 catalysts increase with the loading of Pd varying from 0.5 to 6 wt%. At about 110 °C, the 100 ppm *o*-xylene can be completely oxidized into CO_2 and H_2O over 1% Pd/Al_2O_3 at a GHSV of 10,000 h^{-1}. XRD patterns show that the metallic Pd is considered as the active species in the Pd/Al_2O_3 catalyst for *o*-xylene catalytic oxidation. A two-pathway mechanism for *o*-xylene complete oxidation over the Pd/Al_2O_3 catalyst was proposed. In the first pathway, 2-methyl benzaldehyde, 1(3H)-isobenzofuranone, phthalate, maleate and surface carboxylate were found as the reaction intermediates. This process probably took placed over the γ-Al_2O_3 support. In the second pathway, the *o*-xylene molecules adsorbed on the metallic Pd were oxidized directly into CO_2 and H_2O through the interaction between the adsorbed *o*-xylene and oxygen.

Acknowledgements

This work was financially supported by the Ministry of Science and Technology of China (2007AA061402) and the National Natural Science Foundation of China (20607029).

References

[1] A.P. Jones, Atmos. Environ. 33 (1999) 4535.
[2] D.H. Phillips, Mutat. Res. Genet. Toxicol. Environ. Mutagen. 443 (1999) 139.
[3] K. Okumura, T. Kobayashi, H. Tanaka, M. Niwa, Appl. Catal. B: Environ. 44 (2003) 325.
[4] M.A. Alvarez-Merino, M.F. Ribeiro, J.M. Silva, F. Carrasco-Marín, F.J. Maldonado-Hódar, Environ. Sci. Technol. 38 (2004) 4664.

[5] D. Andreeva, P. Petrova, J.W. Sobczak, L. Ilieva, M. Abrashev, Appl. Catal. B: Environ. 67 (2006) 237.
[6] C. Zhang, H. He, K.-i. Tanaka, Appl. Catal. B: Environ. 65 (2006) 37.
[7] J.C.-S. Wu, Z.-A. Lin, F.-M. Tsai, J.-W. Pan, Catal. Today 63 (2000) 419.
[8] M.-F. Luo, M. He, Y.-L. Xie, P. Fang, L.-Y. Jin, Appl. Catal. B: Environ. 69 (2007) 213.
[9] J.J. Li, X.Y. Xu, Z. Jiang, Z.P. Hao, C. Hu, Environ. Sci. Technol. 39 (2005) 1319.
[10] H.S. Kim, T.W. Kim, H.L. Koh, S.H. Lee, B.R. Min, Appl. Catal. A: Gen. 280 (2005) 125.
[11] P. Dégé, L. Pinard, P. Magnoux, M. Guisnet, Appl. Catal. B: Environ. 27 (2000) 17.
[12] J. Tsou, L. Pinard, P. Magnoux, J.L. Figueiredo, M. Guisnet, Appl. Catal. B: Environ. 46 (2003) 371.
[13] P. Gélin, M. Primet, Appl. Catal. B: Environ. 39 (2002) 1.
[14] A.L. Marsh, D.J. Burnett, D.A. Fischer, J.L. Gland, J. Phys. Chem. B 107 (2003) 12472.
[15] A.L. Marsh, J.L. Gland, Surf. Sci. 536 (2003) 145.
[16] J. Lichtenberger, M.D. Amiridis, J. Catal. 223 (2004) 296.
[17] M. Selvaraj, T.G. Lee, Microporous Mesoporous Mater. 85 (2005) 39.
[18] T.F. Garetto, C.R. Apesteguía, Appl. Catal. B: Environ. 32 (2001) 83.
[19] M. Paulis, H. Peyrard, M. Montes, J. Catal. 199 (2001) 30.
[20] H. Karhu, A. Kalantar, I.J. Vayrynen, T. Salmi, D.Y. Murzin, Appl. Catal. A: Gen. 247 (2003) 283.
[21] M.S. Chen, D.W. Goodman, Catal. Today 111 (2006) 22.
[22] M. Haruta, M. Daté, Appl. Catal. A: Gen. 222 (2001) 427.
[23] S. Zheng, A. Jentys, J.A. Lercher, J. Catal. 241 (2006) 304.
[24] O. Marie, F. Thibault-Starzyk, P. Massiani, J. Catal. 230 (2005) 28.
[25] M. Jang, S.R. McDow, Environ. Sci. Technol. 31 (1997) 1046.
[26] M. Wojciechowska, S. Lomnicki, W. Gut, Catal. Lett. 20 (1993) 305.
[27] O. Klug, W. Forsling, Langmuir 15 (1999) 6961.
[28] X. Zhang, H. He, Z. Ma, Catal. Commun. 8 (2007) 187.
[29] V. Ermini, E. Finocchio, S. Sechi, G. Busca, S. Rossini, Appl. Catal. A: Gen. 190 (2000) 157.
[30] A.M. Turek, I.E. Wachs, E. DeCanio, J. Phys. Chem. 96 (1992) 5000.
[31] S. Krishnamoorthy, J.A. Rivas, M.D. Amiridis, J. Catal. 193 (2000) 264.
[32] J. Baltrusaitis, J.H. Jensen, V.H. Grassian, J. Phys. Chem. B 110 (2006) 12005.
[33] M. Skotak, Z. Karpiński, W. Juszczyk, J. Pielaszek, L. Kepiński, D.V. Kazachkin, V.I. Kovalchuk, J.L. d'Itri, J. Catal. 227 (2004) 11.
[34] A. Jentys, H. Tanaka, J.A. Lercher, J. Phys. Chem. B 109 (2005) 2254.
[35] W.-K. Chen, M.-J. Cao, S.-H. Liu, Y. Xu, J.-Q. Li, Chem. Phys. Lett. 407 (2005) 414.
[36] A.F. Lee, K. Wilson, R.M. Lambert, A. Goldoni, A. Baraldi, G. Paolucci, J. Phys. Chem. B 104 (2000) 11729.